ALMA Memo 594

Flux Density Models for Solar System Bodies in CASA

Bryan Butler
NRAO
November 30, 2012

1. Introduction

CASA 4.0 introduces a modification to the way that the flux densities of solar system bodies are calculated, in order to use them for setting the flux density scale in ALMA observations. The bodies included are: Venus, Mars, Jupiter, Uranus, Neptune, Io, Europa, Ganymede, Callisto, Titan, Ceres, Vesta, Pallas, and Juno. These models may be extended to work for other wavelengths (particularly for VLA), but for now they should only be used for ALMA. The main difference from how it was done previously in CASA is in the brightness temperature models for these bodies, but there is also a change in the way that their sky brightness model is calculated, since *setjy* no longer writes directly into the deprecated MODEL column. This memo describes how the previous flux densities were calculated, and how that has changed in CASA 4.0. The new models are called "Butler-JPL-Horizons 2012" while the old ones were called "Butler-JPL-Horizons 2010". Many of the "models" in the 2010 version were not true models at all, but rather put in by CASA programmers with little to no oversight. This has been remedied in the 2012 versions, for all supported bodies (though the asteroids are still poorly modeled). The detailed description for each body in Appendix A describes the provenance of its model.

2. Generation of Expected Flux Densities

In order to derive the scaling factor to apply to a given collection of visibilities to get them on a true flux density scale (in Janskys), we can observe a source of "known" flux density and structure (the sky brightness distribution is known, in real irradiance units and is given by $I(l,m)$ for sky coordinates l and m). There is always some uncertainty in how well known the flux density from that source is, but hopefully it is within the requirement for ALMA (5% absolute calibration). There is also always some uncertainty in structure, but for many sources that uncertainty is small. Given the known sky brightness distribution, the visibility function can be calculated at the *u,v* locations of the visibilities in a given observation, and the ratio of the expected to the measured visibilities is the scaling factor needed. So, for the i^{th} visibility:

$$V_i = \iint A(l,m)I(l,m)e^{-i2\pi(u_i l + v_i m)}dldm$$

where $A(l,m)$ is the primary beam response. In what follows, we will assume that this is a small field of view, so the sky is planar and also that the body is much smaller than the primary beam, so that the antenna response can be ignored.

2.1 Sky Brightness Distribution and Visibility Function

Eventually, we may want to explicitly be able to allow a full sky brightness distribution $I(l,m)$, and have CASA internally do the above integral by creating a discretized version of that distribution and doing the DFT to derive the visibilities. We are not prepared to do that at this point, however, so have chosen sky brightness distributions that are close enough to reality to give reasonable results, and yet allow the integral to be solved analytically.

For large enough solar system bodies, which are roughly circular (even if elliptical, a change of coordinates can be made to make them so – see below), and assuming a particular form of the limb-darkening such that the sky brightness is: $I = I_0 \cos^n\theta = I_0(1-\rho^2)^{n/2}$ with incidence angle θ and normalized apparent radius $\rho = r/\hat{R}$ for sky coordinate $r = \sqrt{l^2+m^2}$ and apparent body radius $\hat{R}$ ($\hat{R} = R/D$ for body physical radius R and distance D). Then we can explicitly solve the integral equation, yielding for the i^{th} visibility:

$$V_i = V_0 \Lambda_\eta(2\pi\beta_i)$$

where V_0 is the zero-spacing flux density, $\eta = 1 + n/2$, $\beta_i = \hat{R}\sqrt{u_i^2+v_i^2}$ (u_i and v_i in wavelengths), and Λ is the "Lambda function" (Abramowitz & Stegun 1965):

$$\Lambda_\eta(z) = \Gamma(\eta+1)\left(\frac{2}{z}\right)^\eta J_\eta(z)$$

where Γ is the standard Gamma function, and $J_\eta(z)$ is the standard Bessel function of order η and argument z (see Butler and Bastian 1999, or Butler 1994 for more detail). Note that these are functions of both time and frequency. We are also not prepared to implement this right now in CASA either, since we don't have this functional form supported internally. What we **can** do is make the further simplification that there is no limb-darkening, so that $n = 0$, and $\eta = 1$, and we have the "uniform disk" that **is** currently supported internally in CASA:

$$V_i = 2\,V_0\,\mathrm{jinc}(2\pi\beta_i)$$

For zero-spacing flux density V_0. This will deviate from the true brightness visibility function as the spacings get longer, so one implication of this implementation is that baselines that are beyond roughly the half-power point of the visibility function should be used with extreme caution. This happens when the value of β is roughly 0.35. Given this, and the body geometry, the antenna spacing (baseline length, B) at which this is true is given by:

$$B \sim \frac{0.35\,\lambda\,D}{R}$$

for wavelength λ. This is, for example, about 40 m for Uranus at 1 mm wavelength. The spacing of the first null is roughly 1.7 times this length ($\beta \sim 0.61$), or about 70 m for the same example (Uranus at 1 mm).

2.2 Extension to Elliptical Sources

Since many solar system bodies are not circular, but rather elliptical (notably the giant planets), we must account for this. This is trivially done by a simple change of coordinates when calculating $\hat{R}$: $\hat{R} = \sqrt{R_e^2 \cos\kappa + R_p^2 \sin\kappa}\,/D$ for equatorial radius R_e and polar radius R_p and North Polar Position Angle κ.

2.3 The Zero-Spacing Flux Density

The zero-spacing flux density is given by:

$$V_0(\nu, t) = \frac{2h\nu^3}{c^2}\frac{\pi R_m^2}{D^2}\left[\frac{1}{e^{h\nu/kT_b} - 1} - \frac{1}{e^{h\nu/kT_{bg}} - 1}\right]$$

for speed of light c, Planck's constant h, Boltzmann's constant k, mean physical radius R_m (see discussion below), distance to body D, disk-averaged brightness temperature T_b, and background temperature T_{bg}. The brightness temperature can be a function of time and frequency, and the radius and diameter are functions of time. Strictly speaking the background temperature can be a function of time as well, because solar system bodies are moving against the fixed background and the background temperature is a function of position on the sky, but the variation over a particular observation should be small, so can be ignored. The background temperature is a strong function of frequency and position on the sky, however, so eventually that should be included, but until we have access to the accurate Planck mission all-sky maps at mm/sub-mm wavelengths it is premature to assume we can know the distribution, so we should just assume the microwave background temperature of 2.72 K. This will cause problems especially for observations near the galactic plane, which unfortunately solar system bodies often are. When we do have the Planck all-sky maps we can consider trying to use them to estimate T_{bg} more accurately. At sky positions away from the galactic plane, the T_{bg} is small, and the correction is minor (fractions of %, even at 100 GHz), but since we know how to do it the correction is included.

2.4 The Disk-Averaged Brightness Temperature

Until we have the capability of specifying a full sky brightness model, all of the physics of the planetary emission model is entirely contained in a single value, T_b. Fortunately, we can for any brightness distribution, calculate the equivalent T_b that would provide the same whole-disk brightness – i.e., the zero-spacing visibility will still be correct. Where we truly suffer from inability to specify the full sky brightness distribution is in the calculation of the visibility function, or how the visibility amplitude varies with u and v. Appendix A contains details for how T_b is calculated or specified as a function of time and frequency for each body supported in the new models.

3. Implementation in CASA

The parameters we need to calculate the expected flux density for a planet are:

- Planet name
- Time (in MJD)
- Frequency range
- Observatory name

Given these, we can determine:

- Body information: major and minor diameters and position angle (needed to calculate β_i); sky coordinates; topocentric velocity (for doppler shift)
- Observatory information (for doppler shift)
- Zero-spacing visibility, V_0

And we can then proceed with a way of describing the model in CASA and then a way of applying that model to observations to get a scaling factor.

3.1 Body Information

Given the equatorial and polar radii for a body, R_e, and R_p, its distance, D, its sub-Earth latitude, ϕ, and its North Polar Position Angle, κ (measured CCW, or East from North), the major and minor diameters (in arcseconds) and position angle are given by:

$$B_{maj} = 2\,a\frac{R_e}{D}$$

$$B_{min} = 2\,a\frac{R_p^{'}}{D}; \quad R_p^{'} = \sqrt{R_e^2\sin^2\phi + R_p^2\cos^2\phi}$$

$$PA = \kappa$$

where $R_p^{'}$ is the apparent polar radius and a is the conversion factor from radians to arcseconds. Note that $R_m = \sqrt{R_{eq}R_p^{'}}$.

Given the J2000 right ascension, α, and declination, δ, as strings, a proper CASA "direction" quantity can be created by:

```
dirn = me.direction('J2000',str(α)+'deg',str(δ)+'deg')
```

(assuming α and δ are in degrees).

The information for the observing geometry for all of the bodies as a function of time is contained in CASA tables, that were derived from running the JPL Horizons ephemeris, using the geocenter as the observing location (which at the time it was run was using the DE403 ephemerides for the planets). This includes the right ascension and declination, the distance, the rate of change of distance, and the other physical ephemeris quantities needed. Not all bodies have both the polar and equatorial radius in their CASA tables; for those that don't, a mean radius is used.

Given the geocentric radial velocity of the body at the time of observation, and the name of the observatory, we set up a frame in CASA to calculate the doppler shift to apply before calculating the model (since the models are a function of frequency). We do this with the following steps:

```
me.doframe(me.observatory(observatory))
me.doframe(me.epoch('utc',str(MJD)+'d'))
me.doframe(dirn)
rv = me.radialvelocity('geo',str(RadVel)+'km/s')
f0' = me.tofrequency('topo',
     me.todoppler('optical',me.measure(rv,'topo')),
     me.frequency('topo',str(f0)+'Hz'))['m0']['value']
f1' = me.tofrequency('topo',
     me.todoppler('optical',me.measure(rv,'topo')),
     me.frequency('topo',str(f1)+'Hz'))['m0']['value']
f0 = 2 * f0 – f0'
f1 = 2 * f1 – f1'
```

where `f0` is the original lower frequency and `f1` is the original upper frequency of the frequency range, `RadVel` is the geocentric radial velocity, `MJD` is the time (day + fraction), and `observatory` is the observatory name.

3.2 The Zero-Spacing Visibility

Given the distance and mean radius, the zero-spacing visibility can be calculated using the equation above (section 2.3) if the brightness temperature of the body is known. Appendix A below describes the models for the various supported bodies, as a function of frequency.

3.3 The CASA Function to calculate V_o, B_{maj}, B_{min}, κ, and dirn

This is implemented as a python function that can be called with a body name, a list of MJD times, a list of frequency ranges, and an observatory name, and will return, for each time and frequency range the zero-spacing flux density, the estimated error on that flux density, the major and minor axes and position angle, and the direction (the geometries are only returned one-per-time, since they are not frequency-dependent). A status is also returned, indicating success or various error conditions. For now, the errors estimates are all set to 0. In order to estimate the brightness temperature integrated over the input frequency range, a simple summation is done over the tabulated model values in that range (see Appendix A for more information on the brightness temperature models). A doppler correction to the frequency range is made by converting the geocentric velocity to a topocentric velocity as described above (which is why the observatory name is needed). An example call to this python function is:

```
solar_system_fd('Uranus',[56018.232,56018.273],
  [[224.234567e9,224.236567e9],[224.236567e9,224.238567e9]],
  'ALMA')
```

which returns:

```
 [[[0, 0], [0, 0]],
 [[28.629813840109204, 28.630298104324929],
  [28.629997418897673, 28.630481686159907]],
 [[0.0, 0.0], [0.0, 0.0]],
 [[3.3461091470385442, 3.2693917496378404,
254.51323769043466],
  [3.3461211084303302, 3.2694034367866753,
254.51338545729834]],
 [{'m0': {'unit': 'rad', 'value': 0.081157802002122442},
   'm1': {'unit': 'rad', 'value': 0.022025017846591329},
   'refer': 'J2000',
   'type': 'direction'},
  {'m0': {'unit': 'rad', 'value': 0.081195113647730022},
   'm1': {'unit': 'rad', 'value': 0.022041113301227554},
   'refer': 'J2000',
   'type': 'direction'}]]
```

3.4 Describing the Model in CASA

Given zero-spacing visibility, major and minor axes and position angle, and the direction, a `componentlist` can now be created via:

```
cl.addcomponent(flux=V_o, fluxunit='Jy',
     polarization='Stokes', dir=dirn, shape='disk',
     majoraxis= B_maj, minoraxis= B_min, positionangle= κ,
     freq= (f_o + f_1)/2, spectrumtype='spectral index',
     index=+2.0)
```

We note that this kind of spectral model is not strictly true, because the spectrum is really a Planckian one (and a spectral index of +2 would imply Rayleigh-Jeans), but the model is typically run for narrow bandwidths, over which this assumption will not cause excessive error.

3.5 Applying the Model

Once the model is created in a form of a `componentlist`, it can be stored to the MS via:

```
im.ft(complist=componentlist_label)
```

This will Fourier transform the `componentlist` to model visibilities per spectral window. In CASA 4.0, by default only the parameters are stored in the header of the MS and actual model visibilities are evaluated on the fly when it is used. An option to switch to store the model visibilities on disk is available and in that case, MODEL_DATA column is filled.

3.6 How this is used in practice

The Python functions described above are integrated into the *setjy* task for general users in CASA. The flux density models described in this memo are specified by setting the task parameter `standard='Butler-JPL-Horizons 2012'`. Other *setjy* task parameters provide further user specified control over how a subset of the MS is used to set the model. The body name is set via the `field` parameter. In CASA 4.0, each execution of *setjy* causes the model to be calculated and set for only a single time (the centroid time of the selected data). If the body moves significantly during the course of the observation, it will be required to run multiple executions of *setjy* with `selectdata=True` and subsets of the observation selected via appropriate setting of the `timerange` or `scan` parameters. This may change in the future, but it will be a relatively straightforward change in the software, since `solar_system_fd()` already takes a list of times. Because of this, only the interface code needs to be modified by setting multiple `componentlists` for multiple time ranges. By default, the flux density is determined for each channel (`scalebychan=True`) otherwise it is determined per spectral window. By default, the scratch column of the MS is not used; this can be changed by setting `usescratch=True`. When `standard='Butler-JPL-Horizons 2012'`, there is an expandable sub-parameter, `useephemdir`. When this is set to `True`, the task finds the direction to the source from the JPL-Horizons ephemeris table in the CASA repository to set the direction for the model `componentlist`. Otherwise it uses the direction stored in the MS.

As an example, a call to *setjy* using the minimum number of parameters (allowing the others to be their default values) is:

```
setjy(vis='2528.ms',field='Uranus',
      standard='Butler-JPL-Horizons 2012')
```

Note that the zero-spacing flux densities are reported in the log when *setjy* is executed.

A. Appendix - Specifics of Brightness Temperature Models

The bodies that are included are the planets Venus, Mars, Jupiter, Uranus and Neptune; the moons Io, Europa, Ganymede, Callisto, and Titan; and the asteroids Ceres, Vesta, Pallas, and Juno. We do not include a model for Mercury because it is too close to the Sun and thus observations of it suffer from solar confusion (and are daytime, by definition). We do not include a model of Saturn because the effect of the rings is difficult to model (see, e.g., Dunn et al. 2005; Dunn et al. 2002; Grossman et al. 1989; Dowling et al. 1987). We do not include a model of Pluto/Charon because not enough is known about its emission currently.

Each body that is included has a file that tabulates the brightness temperature as a function of frequency. The file has only two columns: frequency in GHz, and brightness temperature in K. The only exception to this is for Mars, which varies with time in a way that can be modeled, so the file for Mars has, for each line,

columns for time and the model brightness temperatures at various frequencies (see the Mars section below). These files are all in the CASA repository in the 4.0 release. For each body, we will now describe the models that are used for the "Butler-JPL-Horizons 2010" and "Butler-JPL-Horizons 2012" versions of *setjy*.

A.1 Major Planets

A.1.1 Venus

2010 – T_b is a tabulation of values vs. frequency, from about 300 MHz to 350 GHz, taken from Butler et al. (2001).

2012 – This is very similar to 2010, but a modified atmospheric model was used which extended to higher altitudes, based on the results of Clancy et al. (2012). The difference between the 2010 and 2012 models is tiny.

Future – This model is satisfactory for continuum, but does not account for atmospheric lines (CO, H_2O, HDO, HCl, ClO, etc. – see, e.g., Clancy et al. 2012; Gurwell et al. 2007; Encrenaz et al. 1995; Schloerb et al. 1980). A model should be developed which does account for these atmospheric lines.

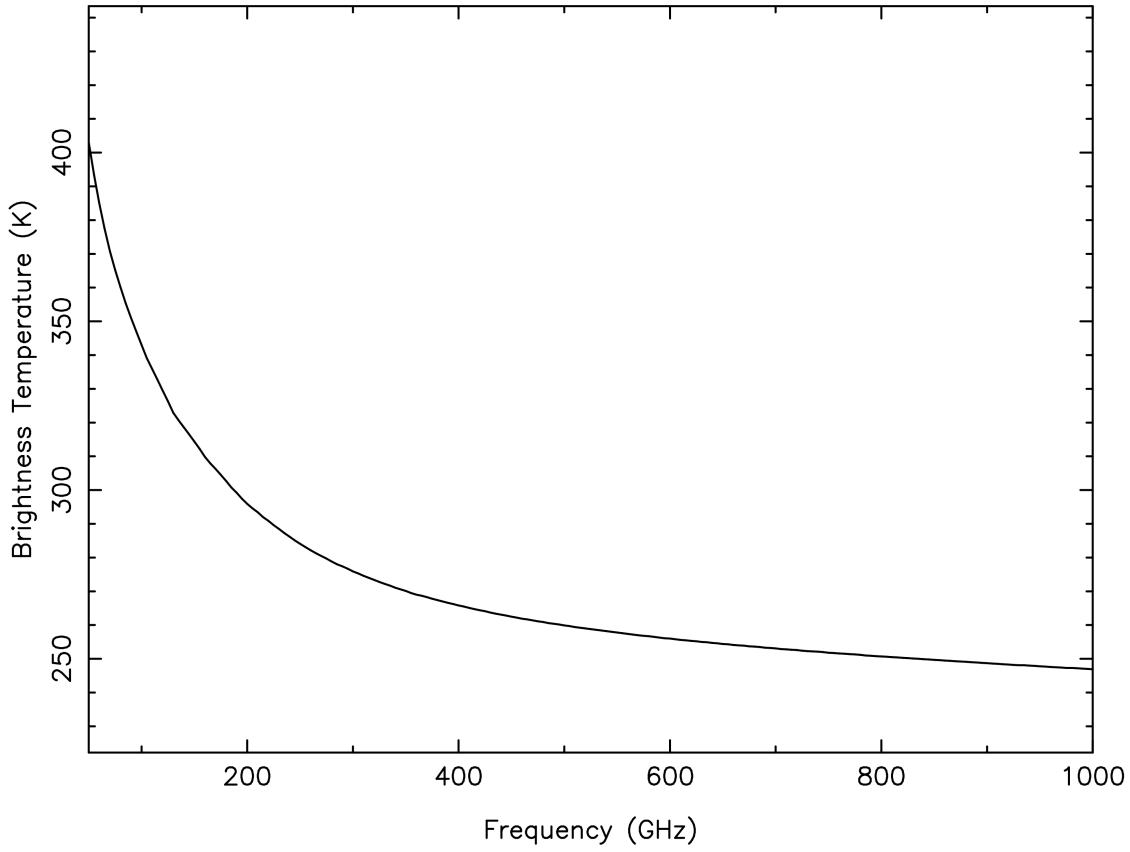

Figure 1. The Butler-JPL-Horizons 2012 CASA model brightness temperature of Venus. The 2010 model values are almost identical so not plotted for comparison.

A.1.2 Mars

2010 – T_b is constant at 210 K.

2012 – A full implementation of the model of Rudy et al. (1987), updated as per http://www.aoc.nrao.edu/~bbutler/work/mars/model. This was calculated as a function of time and frequency, with tabulations every hour and at frequencies of: 30, 80, 115, 150, 200, 230, 260, 300, 330, 360, 425, 650, 800, 950, and 1000 GHz.

Future – This model has a few deficiencies (see the web page), and does not incorporate atmospheric lines (CO, H_2O, H_2O_2, HDO, etc. – see, e.g., Fouchet et al. 2011; Swinyard et al. 2010; Gurwell et al. 2005; Clancy et al. 2004; Encrenaz et al. 2001). It will be difficult to incorporate the atmosphere along with the surface in a proper model, but we can consider doing it in the future.

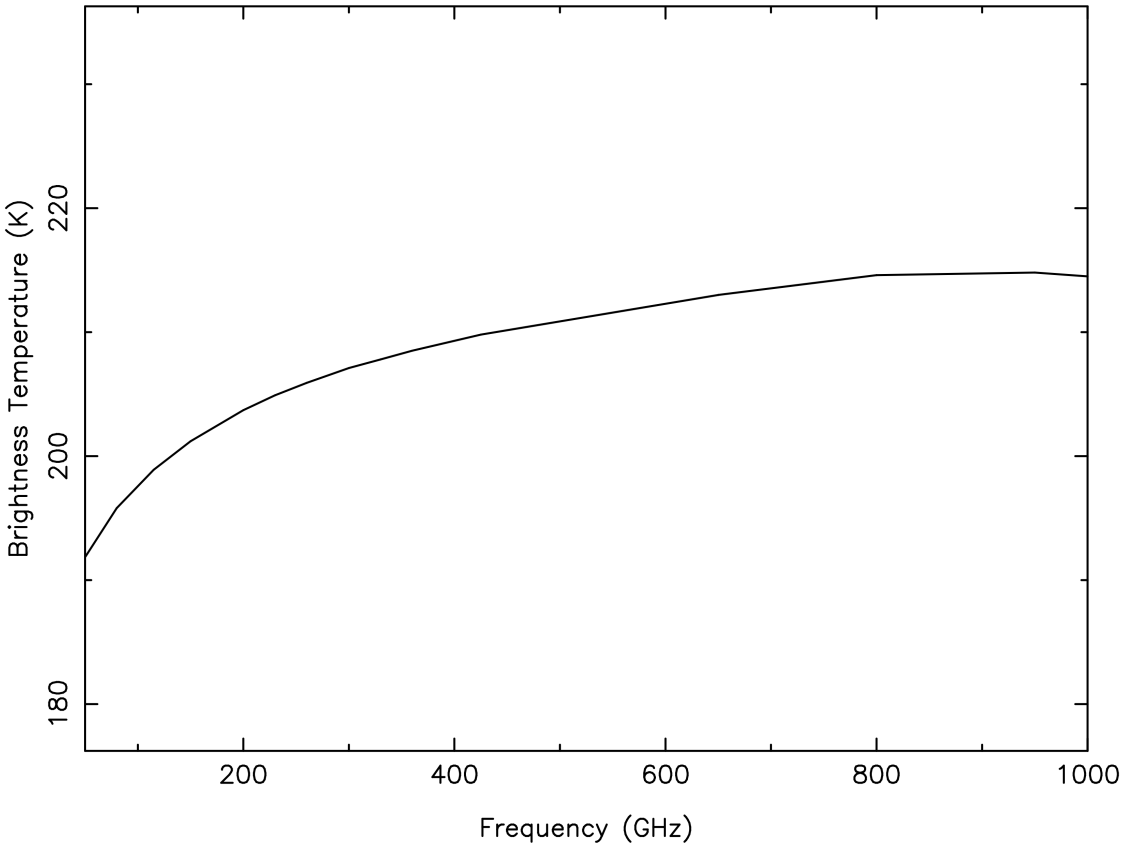

Figure 2. The Butler-JPL-Horizons 2012 CASA model brightness temperature of Mars vs. frequency, for Jan 1, 2010. The 2010 model is constant at 210 K.

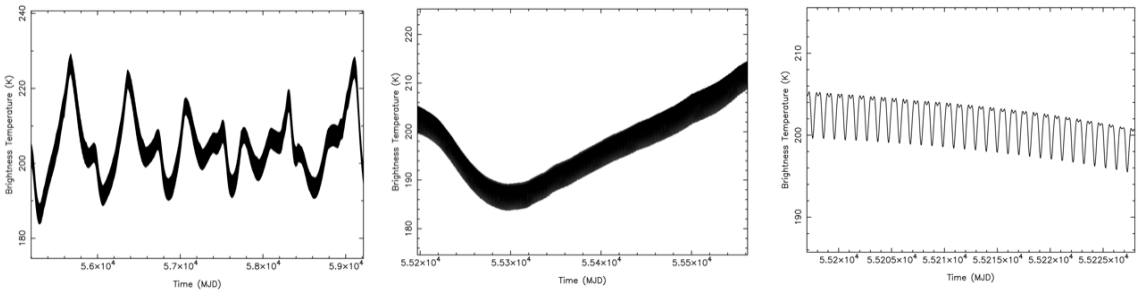

Figure 3. The model brightness temperature of Mars vs. time at 230 GHz. On the left is the entire period from 2010Jan01 to 2020Dec31; in the middle is one year - 2010Jan01 to 2010Dec31; on the right is one month - 2010Jan.

A.1.3 Jupiter

2010 – T_b is a piecewise fit in log-log space to data in de Pater & Massie (1985) from 1mm to 6.2cm, and does not include synchrotron emission.

2012 – Model from Glenn Orton, from 30-1020 GHz. Also contains no synchrotron.

Future – It would be nice to include the synchrotron emission, but for the purposes of ALMA we don't need it, since at wavelengths of 7mm and shorter, the synchrotron is < 1% of the total emission.

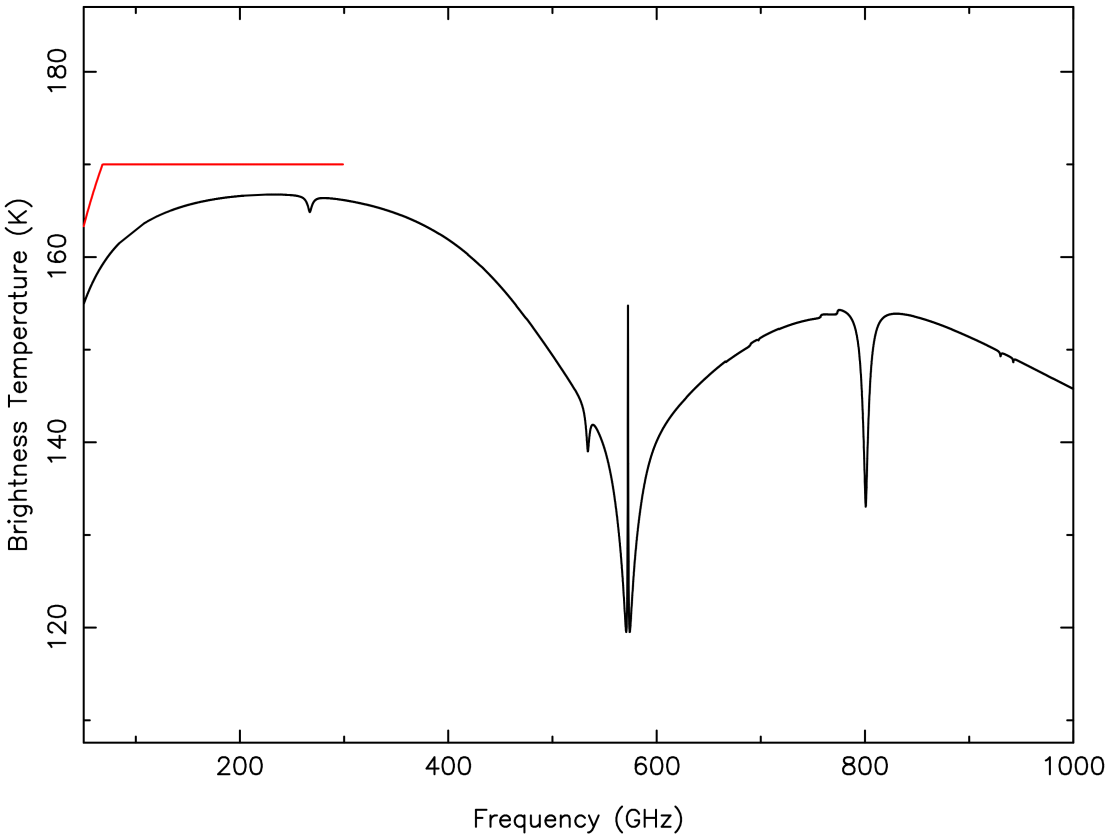

Figure 4. The Butler-JPL-Horizons 2012 CASA model brightness temperature of Jupiter (in black). The 2010 model is shown in red.

A.1.4 Uranus

2010 – T_b is a piecewise fit in log-log space to data in de Pater & Gulkis (1988) from 0.7mm to 6.2cm. There is no ring emission and no synchrotron (but these are negligible effects [if the synchrotron is even there]).

2012 – Model from Glenn Orton and Raphael Moreno, from 60-1800 GHz. Also contains no rings or synchrotron. This model is the so-called "ESA 4" model, which is also used by Herschel for flux density scale calibration.

Future – There is a revision of ESA 4 expected soon, and then a further revision which will incorporate the modeling of Hofstadter et al. (2009) to resolve differences at longer wavelengths. These should be incorporated as they become available. Modeling of the changing disk-averaged brightness temperature as the view of the planet changes (the "north" pole is now visible, and this changes on a ~10 year cycle) should be included eventually.

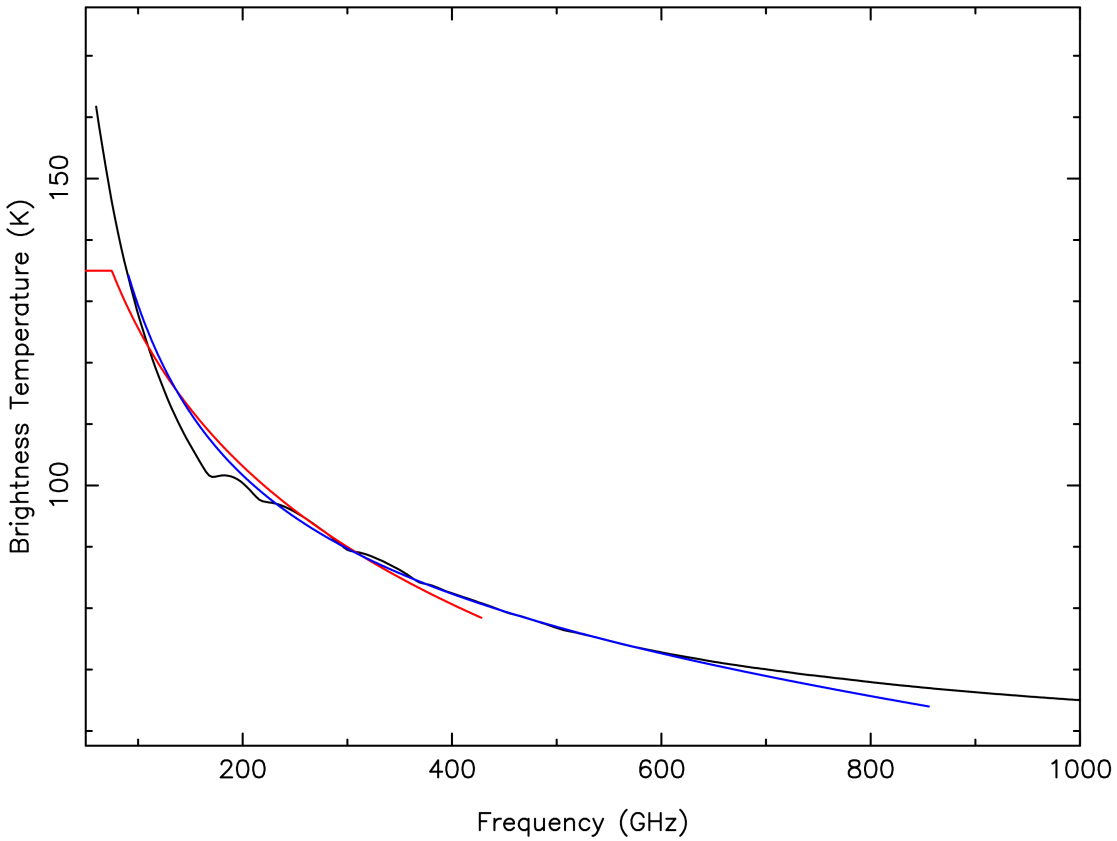

Figure 5. The Butler-JPL-Horizons 2012 CASA model brightness temperature of Uranus (in black). The 2010 model, is shown in red, and blue is the model of Griffin & Orton (1993), used commonly for mm-submm observations.

A.1.5 Neptune

2010 – T_b is a piecewise fit in log-log space to data in de Pater & Richmond (1989) from 0.7mm to 7.5cm. There is no ring emission and no synchrotron (but these are negligible effects [if the synchrotron is even there]).

2012 – Model from Glenn Orton and Raphael Moreno, from 2-2000 GHz. Also contains no rings or synchrotron. This model is the so-called "ESA 3" model, which is also used by Herschel for flux density scale calibration.

Future – There is a revision of ESA 3 expected soon, and then a further revision which will incorporate the modeling of Norwood et al. (2012) to resolve differences at longer wavelengths. These should be incorporated as they become available.

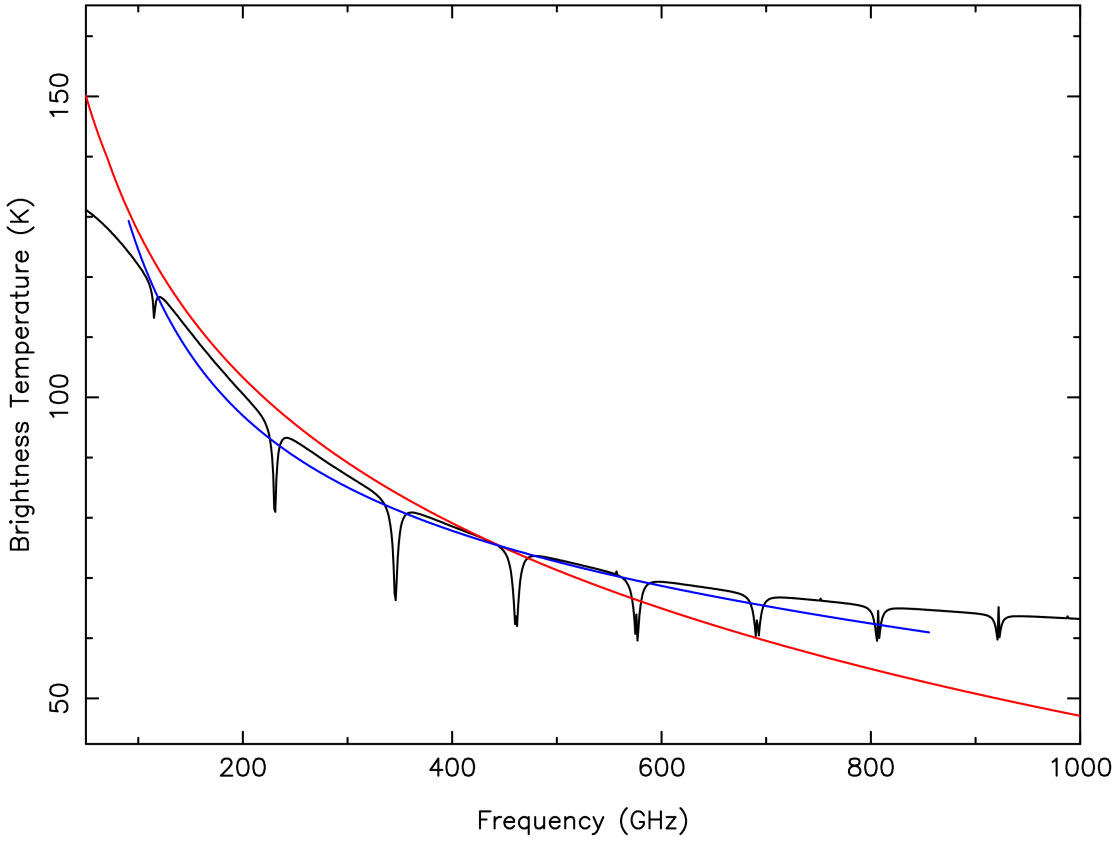

Figure 6. The Butler-JPL-Horizons 2012 CASA model brightness temperature of Neptune (in black). The 2010 model is shown in red, and blue is the model of Griffin & Orton (1993), used commonly for mm-submm observations.

A.2 Satellites (Moons)

A.2.1 Galilean Satellites

The Galilean satellites (Io, Europa, Ganymede, and Callisto) have become common flux density scale calibration sources in recent years, for mm/submm-wavelength interferometers. They are difficult to use for this purpose for single dishes because of the confusion of Jupiter. In fact, this confusion is often also a problem with interferometers, because the emission from Jupiter is so strong that even when it is out in the sidelobes, it causes contamination of the visibilities that must be carefully treated. There have been fairly extensive observations of these bodies in the mm and cm, but because of the confusion from Jupiter, there is no consistent result that extends from the submm to cm wavelengths yet – this is an

open research topic. For instance, the observations of Ulich et al. (1984), Ulich (1981), and Ulich and Conklin (1976) seem much higher than others. Similarly, older VLA observations that have been published (de Pater et al. 1984; Muhleman et al. 1986) do not match more recent re-reductions of those data sets (Butler 2012). We also note that there may be spatial differences in surface properties that will give these bodies thermal lightcurves – but these have not been measured reliably to date. We have therefore chosen to use the following observations in determining the brightness temperature spectrum of the Galilean satellites:

- IR values from Morrison (1977). Note that these actually agree fairly well with the newer Galileo PPR observations (Orton et al. 1996; Rathbun et al. 2004; Rathbun et al. 2010) when you account for a ~10% beaming factor (confirmed with John Spencer in private communication).
- mm/submm values only from the IRAM 30-m and interferometers, so from IRAM, PdBI, SMA, and OVRO.
- cm values only from re-reductions of old VLA data.

Table 1 shows the results of that compilation. We take the data in that table for each body and interpolate with a constrained spline (the function *splrep* from the scipy module in python).

Table 1. Compilation of brightness temperature observations of the Galilean satellites.

Body	Frequency (GHz)	T_b (K)	ΔT_b (K)	Reference
Io	29980	138.0	4.0	[1]
Io	14990	129.0	4.0	[1]
Io	345	95.9	6.0	[2]
Io	225	96.7	7.0	[2]
Io	115	98.2	8.7	[3]
Io	110	97.3	7.0	[2]
Io	43.3	106.4	6.0	[4]
Io	22.46	108.5	5.0	[4]
Io	14.94	105.2	5.0	[4]
Europa	29980	130.0	4.0	[1]
Europa	14990	121.0	4.0	[1]
Europa	340	94.2	3.0	[2]
Europa	224	88.4	5.0	[2]
Europa	115	99.2	9.7	[3]
Europa	43.3	97.2	6.0	[4]
Europa	22.46	108.5	5.0	[4]
Europa	14.9	105.2	5.0	[4]
Ganymede	29980	143.0	4.0	[1]
Ganymede	14990	140.0	5.0	[1]
Ganymede	686	113.9	13.3	[2]
Ganymede	224	98.8	6.0	[2]

Ganymede	224	95.1	7.0	[5]
Ganymede	115	78.3	5.3	[3]
Ganymede	86	89.8	4.7	[5]
Ganymede	43.3	83.5	5.0	[4]
Ganymede	22.46	78.0	4.0	[4]
Ganymede	14.94	77.9	4.0	[4]
Ganymede	4.94	115.3	4.0	[4]
Callisto	29980	154.0	4.0	[1]
Callisto	14990	152.0	4.0	[1]
Callisto	686	128.9	9.2	[2]
Callisto	340	118.0	6.7	[2]
Callisto	276	115.5	5.0	[2]
Callisto	224	117.0	5.0	[2]
Callisto	224	111.6	8.0	[5]
Callisto	115	102.0	5.8	[3]
Callisto	86	111.6	8.0	[5]
Callisto	43.3	104.2	6.0	[4]
Callisto	22.46	103.9	5.0	[4]
Callisto	14.94	101.3	5.0	[4]
Callisto	4.94	108.9	4.0	[4]

[1] Morrison 1977
[2] SMA results from Gurwell & Moullet (personal communication)
[3] Muhleman & Berge 1991
[4] Butler (2012)
[5] Moreno (2007)

A.2.1.1 Io

2010 – T_b is constant at 110 K, taken from Rathbun et al. (2004).

2012 – Model is interpolated as explained above from the observations.

Future – The plot below shows very clearly that the brightness temperature spectrum for Io is very poorly known. Again, this is almost certainly because of the confusion from Jupiter in previous observations. It is **strongly** recommended to not use Io as a primary flux density scale calibrator for ALMA observations until more careful observations are done (with ALMA itself). We note also that Io has narrow atmospheric lines of at least SO_2, SO, and NaCl (Moullet et al. 2010a), but they are so narrow that they will not affect most observations of the body to be used for flux density scale calibration.

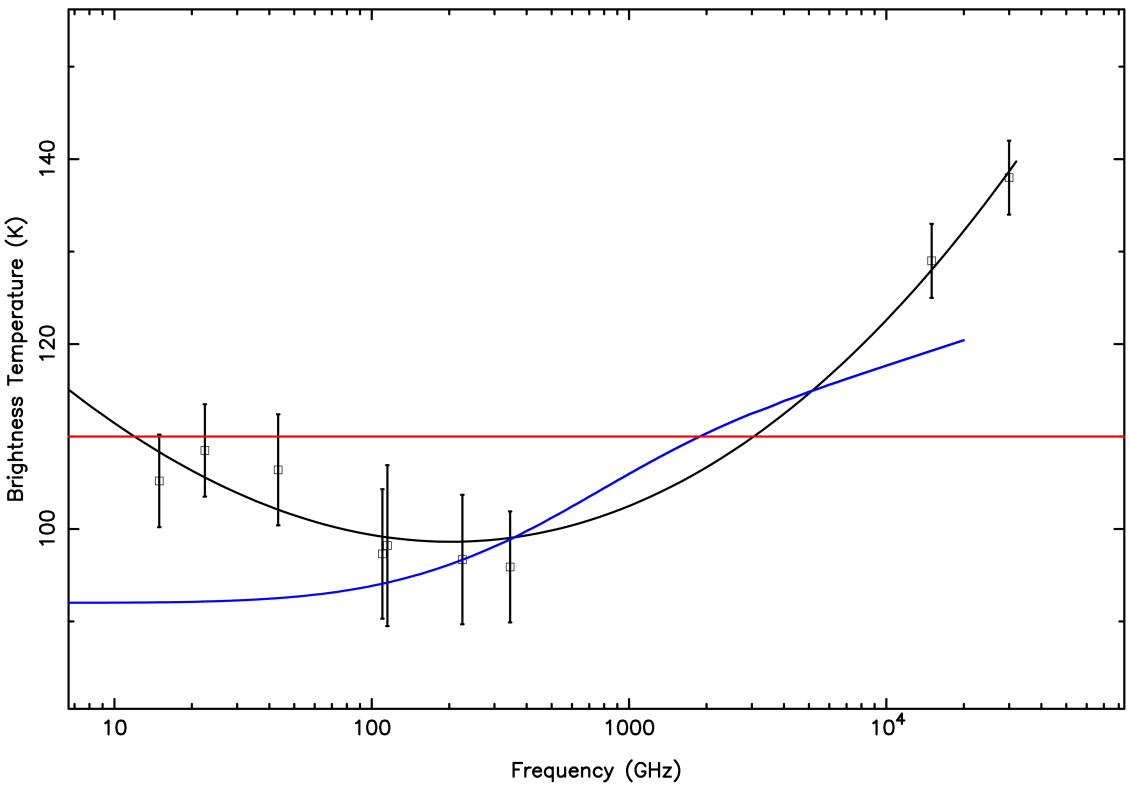

Figure 7. The Butler-JPL-Horizons 2012 CASA model brightness temperature of Io (in black). Data points with error bars from the above table are also shown. The 2010 model is shown in red, and blue is the model of Moreno et al. (2009).

A.2.1.2 Europa

2010 – T_b is constant at 109 K, taken from a NASA web page.

2012 – Model is interpolated as explained above from the observations.

Future – The plot below shows very clearly that, similar to Io, the brightness temperature spectrum for Europa is very poorly known. Again, this is almost certainly because of the confusion from Jupiter in previous observations. It is **strongly** recommended to not use Europa as a primary flux density scale calibrator for ALMA observations until more careful observations are done (with ALMA itself).

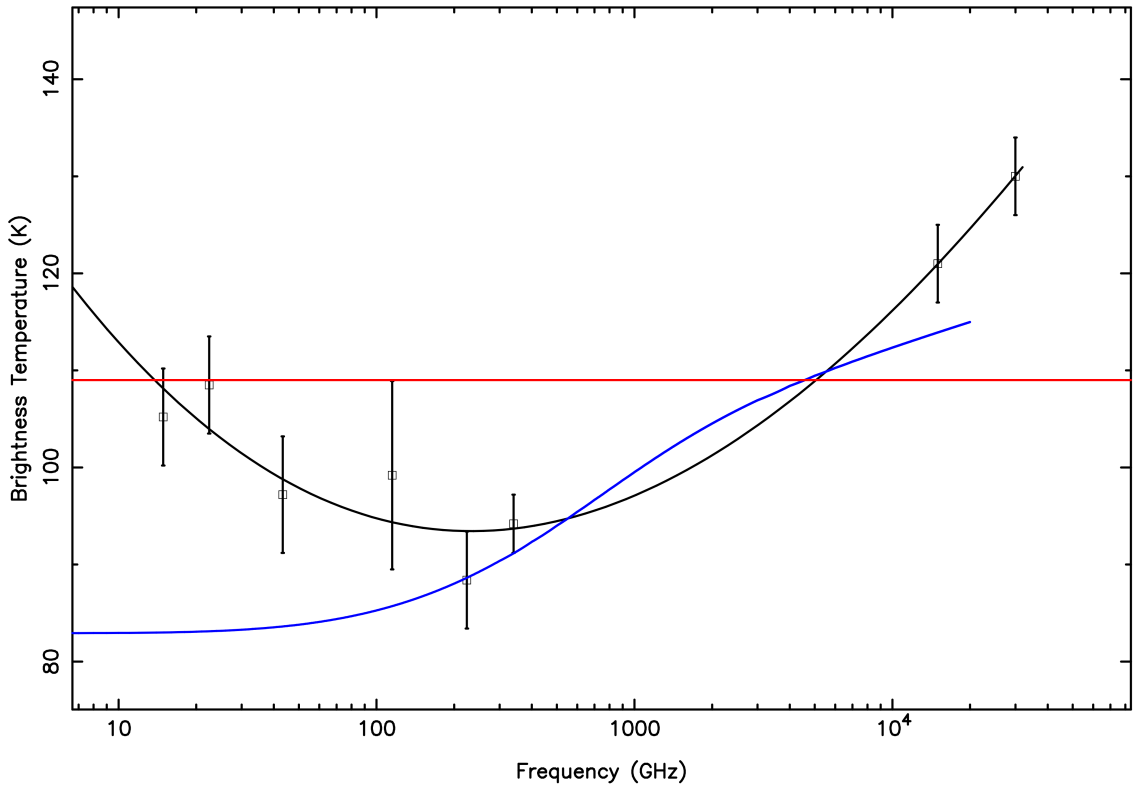

Figure 8. The Butler-JPL-Horizons 2012 CASA model brightness temperature of Europa (in black). Data points with error bars from the above table are also shown. The 2010 model is shown in red, and blue is the model of Moreno et al. (2009).

A.2.1.3 Ganymede

2010 – T_b is constant at 110 K, taken from Delitsky & Lane (1998).

2012 – Model is interpolated as explained above from the observations. The 6-cm point was not used in the spline interpolation of the measurements, as it caused a severe oscillation in the fitting spline.

Future – While the situation for Ganymede is much better than for Io or Europa, there is still some uncertainty in the modeling. It does not have to be avoided like Io and Europa, but further observations, both from ALMA and at cm wavelengths (from the JVLA, probably) will be needed to improve the modeling. At that point, those better models should be used.

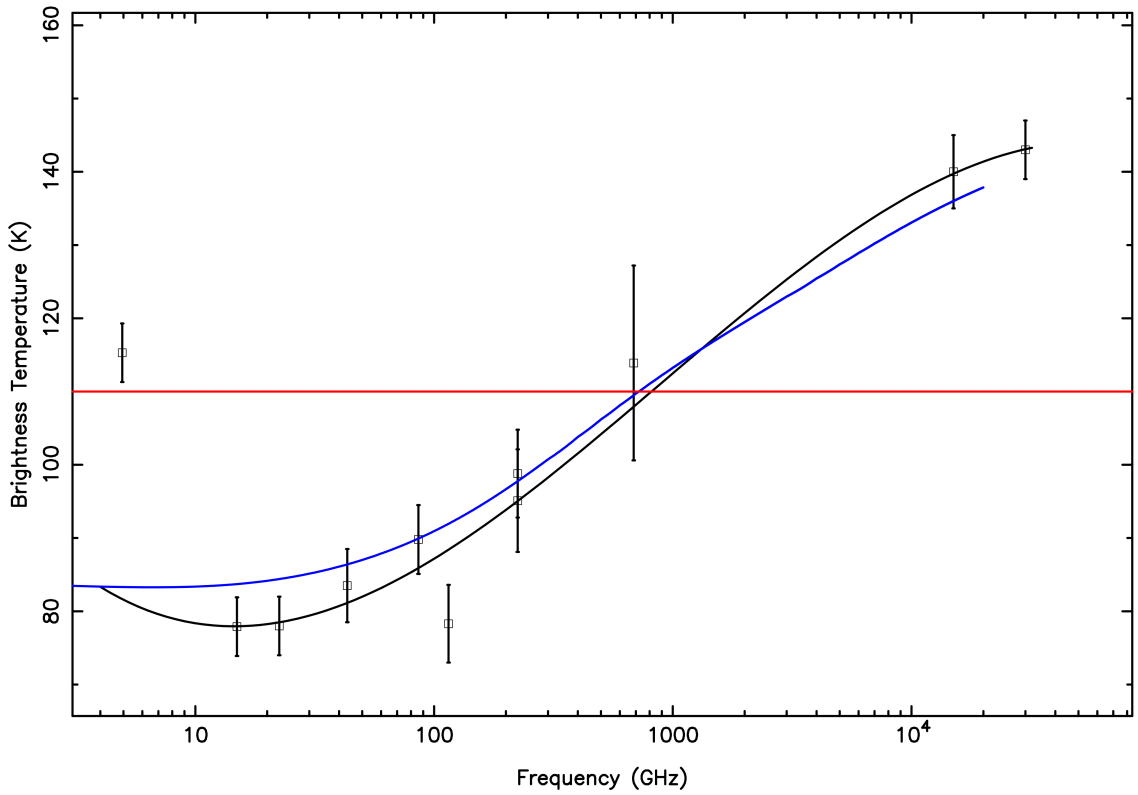

Figure 9. The Butler-JPL-Horizons 2012 CASA model brightness temperature of Ganymede (in black). Data points with error bars from the above table are also shown. The 2010 model is shown in red, and blue is the model of Moreno et al. (2009).

A.2.1.4 Callisto

2010 – T_b is constant at 134 K, taken from Moore et al. (2004).

2012 – Model is interpolated as explained above from the observations.

Future – Callisto is similar to Ganymede - the situation is much better than for Io or Europa, there is still some uncertainty in the modeling. It does not have to be avoided like Io and Europa, but further observations, both from ALMA and at cm wavelengths (from the VLA, probably) will be needed to improve the modeling. At that point, those better models should be used.

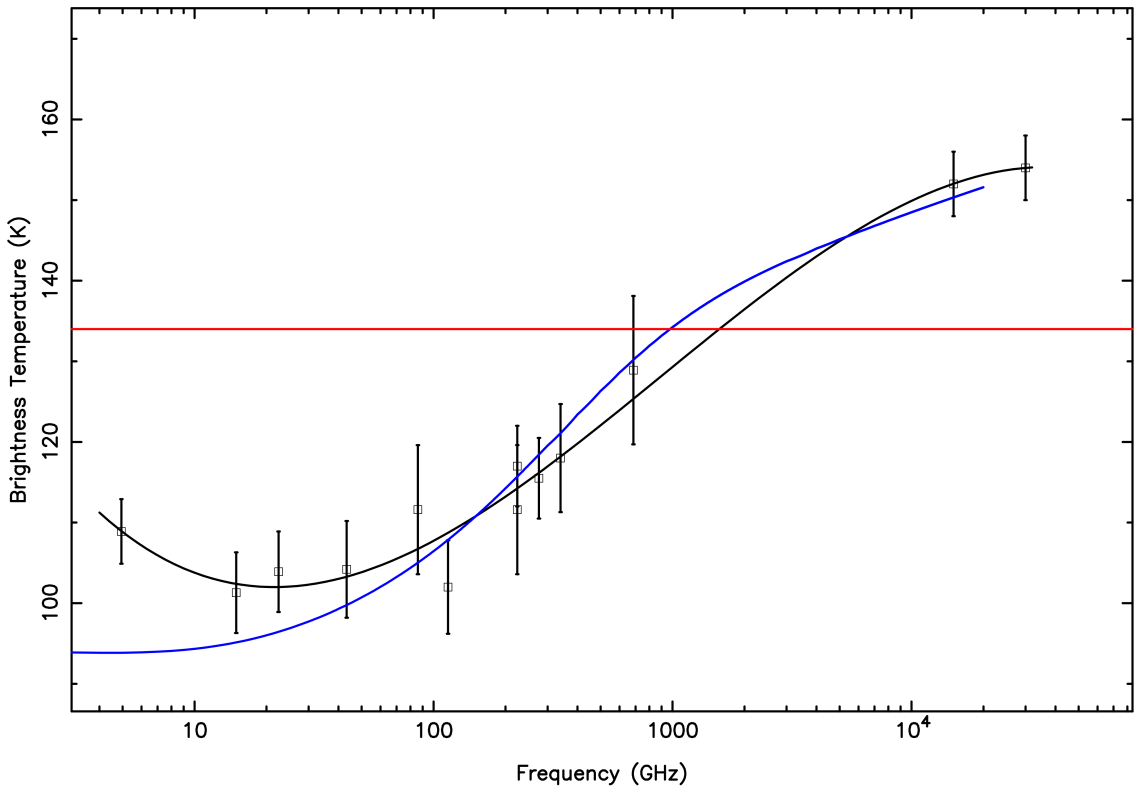

Figure 10. The Butler-JPL-Horizons 2012 CASA model brightness temperature of Callisto (in black). Data points with error bars from the above table are also shown. The 2010 model is shown in red, and blue is the model of Moreno et al. (2009).

A.2.2 Titan

2010 – T_b is constant at 76.6 K, unknown provenance.

2012 – Model from Mark Gurwell, from 53.3-1024.1 GHz. Contains surface and atmospheric emission. The atmosphere includes N_2-N_2 and N_2-CH_4 Collision-Induced Absorption (CIA), and lines from minor species CO, ^{13}CO, $C^{18}O$, HCN, $H^{13}CN$ and $HC^{15}N$. See, e.g., Gurwell & Muhleman (2000); Gurwell (2004);

Future – While Titan can be a very good calibrator at some frequencies, the very bright spectral lines from the atmosphere must be treated with care (see Figures 12 and 13). This model is quite good, but as we measure the atmospheric abundances with ALMA it should be updated. In addition, contributions from CH_3CN and HC_3N should be included.

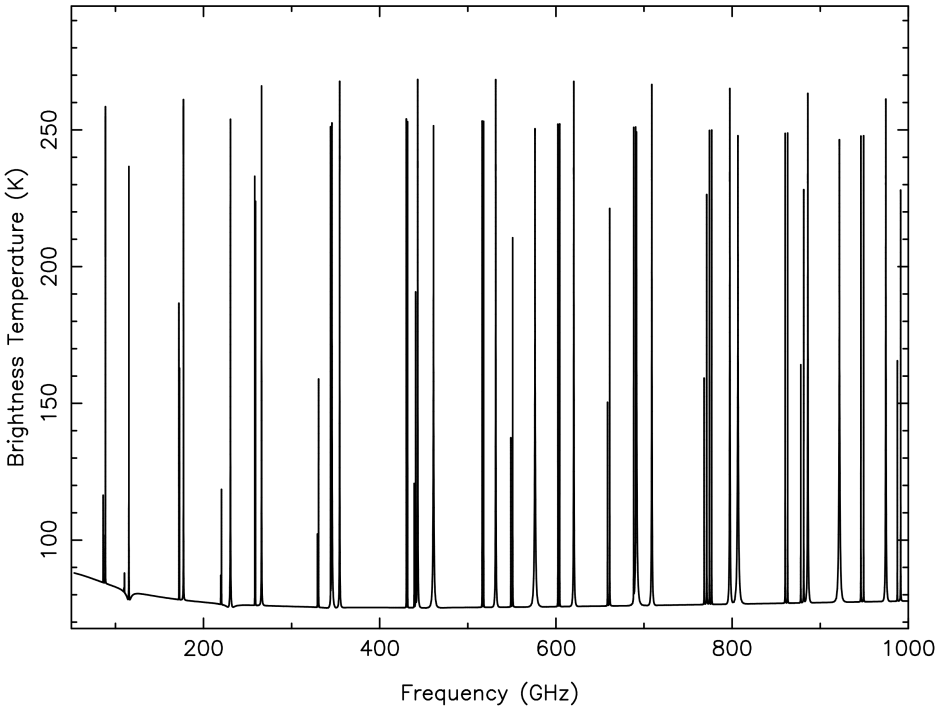

Figure 11. The Butler-JPL-Horizons 2012 CASA model brightness temperature of Titan.

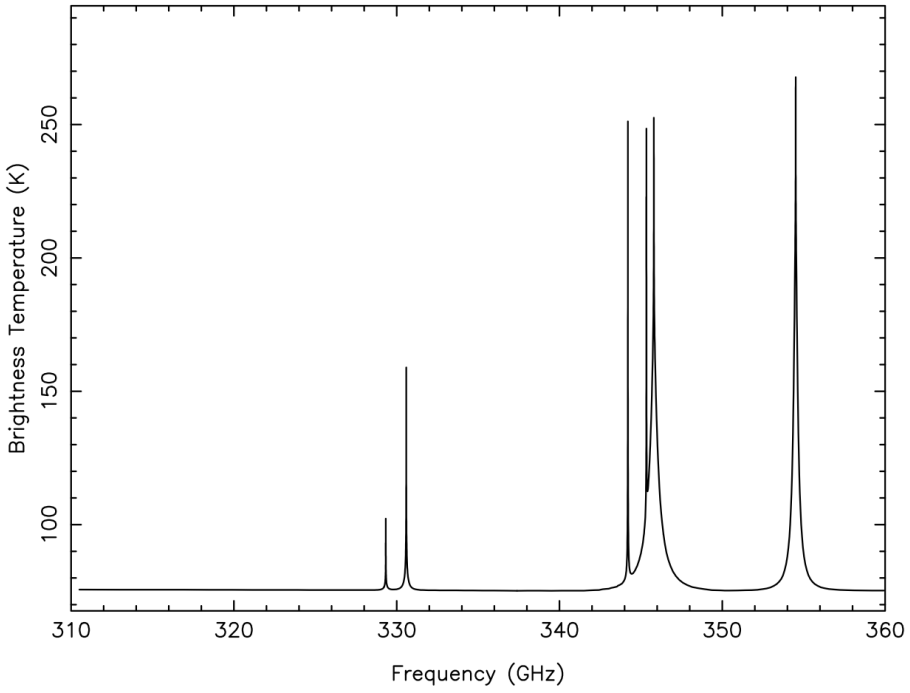

Figure 12. The Butler-JPL-Horizons 2012 CASA model brightness temperature of Titan, zoomed in to part of Band 7. Spectral lines from XX, YY, and ZZ are prominent.

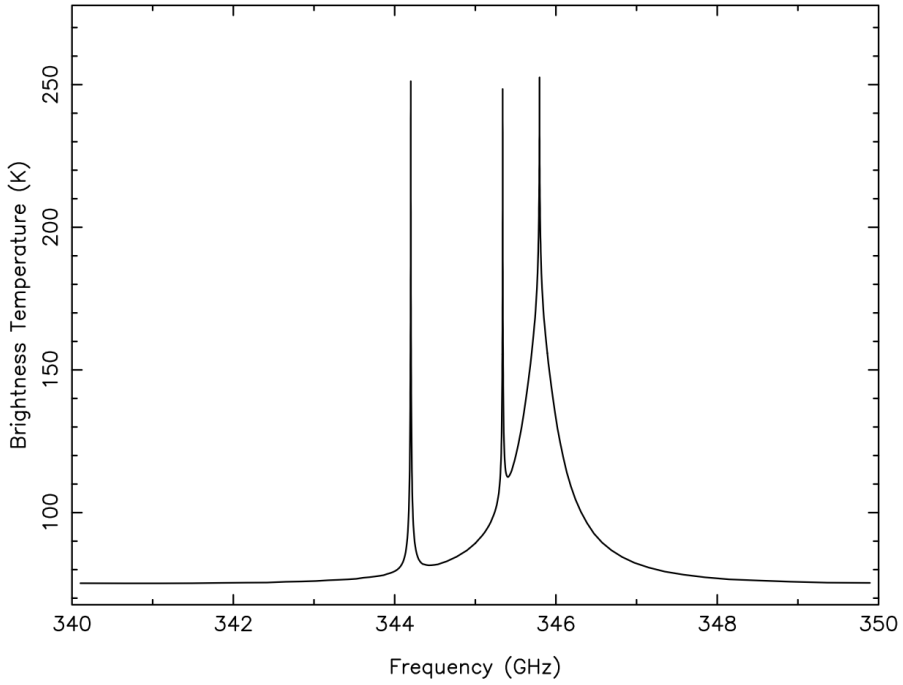

Figure 13. The Butler-JPL-Horizons 2012 CASA model brightness temperature of Titan, zoomed in to roughly the default continuum frequencies for band 7. The CO 3-2 transition is prominent, and demonstrates why care should be exercised when using Titan as a flux density scale calibrator (the situation in Band 6 is similar).

A.3 Asteroids

The models for the asteroids have been only modestly updated in the 2012 models, with the brightness temperature still taken as constant with frequency. This will be a major area to address in the near-future, since models of the asteroids are available from several sources now (see, e.g., Muller & Lagerros 2002; Mueller 2012). Better models should be used, as well as more of the larger asteroids (Hygeia, Europa, Davida, etc.).

A.3.1 Ceres

2010 – T_b is constant at 167 K, taken from Saint-Pe et al. (1993).

2010 – T_b is constant at 185 K, taken from a combination of Moullet et al. (2010b), Muller & Lagerros (2002), Redman et al. (1998), and Altenhoff et al. (1996).

A.3.2 Vesta

2010 – T_b is constant at 160 K, taken from Chamberlain et al. (2009).

2012 – T_b is constant at 155 K, taken from a combination of Leyrat et al. (2012), Chamberlain et al. (2009), Redman et al. (1998), and Altenhoff et al. (1994).

NOTE – Vesta is known to have a large light curve (10's of % – see references above) in the submm and mm, and this will have to be modeled carefully.

A.3.3 Pallas

2010 – T_b is constant at 164 K, unknown provenance.

2012 – T_b is constant at 189 K, taken from a combination of Chamberlain et al. (2009), and Altenhoff et al. (1994).

A.3.4 Juno

2010 – T_b is constant at 163 K, taken from Lim et al. (2005).

2012 – T_b is constant at 153 K, taken from a combination of Chamberlain et al. (2009) and Altenhoff et al. (1994).

Acknowledgements

Credit for the models of the brightness temperatures goes to: Glenn Orton, Raphael Moreno, Mark Gurwell, Arielle Moullet, and Mark Hofstadter. For the actual implementation, credit goes to Tak Tsutsumi, who took the original python code for this and modified it for use in the production version of CASA, as well as implementing the specification of the sky brightness model (as a componentlist) given the expected zero-spacing flux density. Finally, Todd Hunter was invaluable in providing timely testing of the implementation of these models in CASA.

References

Abramowitz, M. & I.N. Stegun 1965. Handbook of Mathematic Functions, Dover

Altenhoff, W.J. et al. 1996. Precise flux density determination of 1 Ceres with the Heinrich-Hertz-Telescope at 250Hz, *A&A, 309,* 953

Altenhoff, W.J. et al. 1994. Millimeter-wavelength observations of minor planets, *A&A, 287,* 641

Butler, B.J. et al. 2001. Accurate and Consistent Microwave Observations of Venus and Their Implications, *Icarus, 154*, 226

Butler, B.J., & T.S. Bastian 1999. Solar System Objects, in *Synthesis Imaging in Radio Astronomy II*, ed. G.B. Taylor, C.L. Carilli, & R.A. Perley, pp. 625-656, ASP Conference Series, 180

Butler, B.J. 1994. 3.5-cm radar investigation of Mars and Mercury: Planetological implications, Ph.D. Thesis, Caltech

Chamberlain, M.A. et al. 2009. Submillimeter photometry and lightcurves of Ceres and other large asteroids, *Icarus, 202,* 487

Clancy, R.T. et al. 2012. Thermal structure and CO distribution for the Venus mesosphere/lower thermosphere: 2001-2009 inferior conjunction sub-millimeter CO absorption line observations, *Icarus, 217*, 779
Clancy, R.T. et al. 2004. A measurement of the 362 GHz absorption line of Mars atmospheric H_2O_2, *Icarus, 168,* 116
de Pater, I. & S. Gulkis 1988. VLA observations of Uranus at 1.3-20 cm, *Icarus, 75,* 306
de Pater, I. & M. Richmond 1989. Neptune's microwave spectrum from 1 mm to 20 cm, *Icarus, 80,* 1
de Pater, I. & S.T. Massie 1985. Models of the millimeter-centimeter spectra of the giant planets, *Icarus, 62,* 143
de Pater, I. et al. 1984. VLA observations of the Galilean satellites, *Icarus, 57,* 93
Delitsky, M.L. & A.L. Lane 1998. Ice chemistry on the Galilean satellites, *JGR, 103,* 31391
Dowling, T.E. et al. 1987. Aperture synthesis observations of Saturn and its rings at 2.7-mm wavelength, *Icarus, 70,* 506
Dunn, D.E. et al. 2005. High-Quality BIMA-OVRO Images of Saturn and its Rings at 1.3 and 3 Millimeters, *AJ, 129,* 1109
Dunn, D.E. et al. 2002. More Microwave Observations of Saturn: Modeling the Ring with a Monte Carlo Radiative Transfer Code, *Icarus, 160,* 132
Encrenaz, T.H. et al. 2001. The water vapor vertical distribution on mars from millimeter transitions of HDO and $H_2{}^{18}O$, *P&SS, 49,* 731
Encrenaz, T.H. et al. 1995. The thermal profile and water abundance in the Venus mesosphere from H_2O and HDO millimeter observations, *Icarus, 117,* 162
Fouchet, T. et al. 2011. Interferometric millimeter observations of water vapor on Mars and comparison with Mars Express measurements, *P&SS, 59,* 683
Griffin, M.J. & G.S. Orton 1993. The near-millimeter brightness temperature spectra of Uranus and Neptune, *Icarus, 105,* 537
Grossman, A.W. et al. 1989. High-resolution microwave images of Saturn, *Science, 245,* 1211
Gurwell, M.A. et al. 2007. SWAS observations of water vapor in the Venus mesosphere, *Icarus, 188*, 288
Gurwell, M.A. et al. 2005. Mars surface and atmospheric temperature during the 2001 global dust storm, *Icarus, 175,* 23
Gurwell, M.A. 2004. Submillimeter Observations of Titan: Global Measures of Stratospheric Temperature, CO, HCN, HC_3N, and the Isotopic Ratios $^{12}C/^{13}C$ and$^{14}N/^{15}N$, *ApJ, 616,* L7
Gurwell, M.A. & D.O. Muhleman 2000. Note: CO on Titan: More Evidence for a well-mixed vertical profile, *Icarus, 145,* 653
Hofstadter, M.D. et al. 2009. Infrared and Microwave Observations of Uranus: Implications for Temperature, Composition, Circulation and a Standard Calibration Model for Herschel, *BAAS, 41,* 28.03
Leyrat, C. et al. 2012. Thermal properties of (4) Vesta derived from Herschel measurements, *A&A, 539,* A154
Lim, L.F. et al. 2005. Thermal infrared (8 13 μm) spectra of 29 asteroids: the Cornell Mid-Infrared Asteroid Spectroscopy (MIDAS) Survey, *Icarus, 173,* 385

Moore, J.M. et al. 2004. Callisto, in *Jupiter*, ed. F. Bagenal, T.E. Dowling, & W.B. McKinnon, pp. 397-426, Cambridge University Press
Moreno, R 2007. Report on continuum measurements of Ganymede and Callisto with the IRAM–PdB interferometer : Application to flux calibration, Internal Memo.
Morrison, D. et al. 1977. Galilean satellites - Anomalous temperatures disputed, *Science, 195,* 90
Morrison, D. & D.P. Cruikshank 1974. Physical Properties of the Natural Satellites, *SSRv, 15,* 641
Moullet, A. et al. 2010a. Simultaneous mapping of SO_2, SO, NaCl in Io's atmosphere with the Submillimeter Array, *Icarus, 208,* 353
Moullet, A. et al. 2010b. Thermal rotational lightcurve of dwarf-planet (1) Ceres at 235 GHz with the Submillimeter Array, *A&A, 516,* L10
Mueller, M. 2012. Surface Properties of Asteroids from Mid-Infrared Observations and Thermophysical Modeling, Ph.D. Thesis, Freie Universitaet Berlin
Muller, T.G. & J.S.V. Lagerros 2002. Asteroids as calibration standards in the thermal infrared for space observatories, *A&A, 381,* 324
Muhleman, D.O. and G.L. Berge 1991. Observations of Mars, Uranus, Neptune, Io, Europa, Ganymede, and Callisto at a wavelength of 2.66 mm, *Icarus, 92,* 263
Muhleman, D.O. et al. 1986. Precise VLA positions and flux-density measurements of the Jupiter system, *AJ, 92,* 1428Orton, G.S. et al. 1996. Galileo Photopolarimeter-Radiometer Observations of Jupiter and the Galilean Satellites, *Science, 274,* 389
Norwood, J. et al. 2012. Modeling the Neptunian Troposphere at Microwave Wavelengths, *BAAS, 44,* 504.05
Rathbun, J.A. et al. 2004. Mapping of Io's thermal radiation by the Galileo photopolarimeter-radiometer (PPR) instrument, *Icarus, 169,* 127
Rathbun, J.A. et al. 2010. Galileo PPR observations of Europa: Hotspot detection limits and surface thermal properties, *Icarus, 210,* 763
Redman, R.O. et al. 1998. High-Quality Photometry of Asteroids at Millimeter and Submillimeter Wavelengths, *AJ, 116,* 1478
Rudy, D.J. et al. 1987. Mars - VLA observations of the northern hemisphere and the north polar region at wavelengths of 2 and 6 cm, *Icarus, 71,* 159
Saint-Pe, O. et al. 1993. Ceres surface properties by high-resolution imaging from earth, *Icarus, 105,* 271
Schloerb, F.P. et al. 1980. Observations of CO in the stratosphere of Venus via its J=0-1 rotational transition, *Icarus, 43,* 121
Swinyard, B.M. et al. 2010. The Herschel-SPIRE submillimetre spectrum of Mars, *A&A, 518,* L151
Ulich, B.L. et al. 1984. Planetary observations at a wavelength of 1.32 mm, *Icarus, 60,* 590
Ulich, B.L. 1981. Millimeter-wavelength continuum calibration sources, *AJ, 86,* 1619
Ulich, B.L. & E.K. Conklin 1976. Observations of Ganymede, Callisto, Ceres, Uranus, and Neptune at 3.33 MM wavelength, *Icarus, 27*, 183